Dalton Transactions

ROYAL SOCIETY OF CHEMISTRY

PAPER

View Article Online
View Journal | View Issue

Cite this: *Dalton Trans.*, 2026, **55**, 152

Fluorinated B-phenylated scorpionates as tunable platforms for stabilizing thallium(I) and silver(I)–ethylene complexes

Anurag Noonikara-Poyil, [a] Vo Quang Huy Phan, [a] Mukundam Vanga, [a] Andrii Boretskyi,[b] Pavel Mykhailiuk *[b,c] and H. V. Rasika Dias *[a]

Received 20th November 2025,
Accepted 3rd December 2025

DOI: 10.1039/d5dt02782a

rsc.li/dalton

Fluorinated and B-phenylated bis(pyrazolyl)borate and bis(pyridyl)borate ligands have been utilized in thallium(I) and silver(I)–ethylene chemistry. These ligands contain electron-withdrawing trifluoromethyl or pentafluorosulfanyl groups that create a chemically inert half-rim and, together with a flanking phenyl group, provide steric protection at the metal site. Thallium(I) complexes display κ^2-N,N ligand binding and noteworthy Tl–F coupling in ^{19}F NMR, indicating proximity effects of the fluorinated substituents. The silver–ethylene complexes $[Ph_2B(3\text{-}(CF_3)Pz)_2]Ag(C_2H_4)$, $[Ph_2B(3\text{-}(SF_5)Pz)_2]Ag(C_2H_4)$, and $[Ph_2B(6\text{-}(CF_3)Py)_2]Ag(C_2H_4)$ feature trigonal-planar silver(I) sites, with NMR data showing upfield shifts for ethylene proton and carbon resonances relative to those of the free ethylene. The steric effects of fluorinated supporting ligands in thallium and silver complexes were evaluated using buried-volume calculations. In addition, C–H activation of alkanes *via* carbene insertion catalyzed by silver complexes is reported. Overall, the findings illustrate how fluorinated groups and N-heterocyclic donor arms influence metal–ligand bonding, the stability of coinage-metal π-complexes, and influence the catalytic efficiency and selectivity in alkane C–H functionalization.

Introduction

Bis(pyrazolyl)borates are useful monoanionic, nitrogen donor site-based ligands,[1,2] which can be tuned electronically and sterically to support transition metals in various applications, such as catalysis, bioinorganic chemistry, and the development of luminescent materials.[3] Bis(pyridyl)borates are a related ligand family, but they are based on larger, six-membered pyridyl heterocycles instead of five-membered pyrazolyl groups. Although bis(pyridyl)borates have been known since the 1990s,[4,5] they have received less attention in metal coordination chemistry compared to their bis(pyrazolyl)borate counterparts.[4,6–17] Moreover, bis(pyridyl)borates with pyridyl ring substituents near metal coordination sites were unknown until recently.[11,12,18] We are interested in developing fluorinated versions of both these ligand classes,[11,12,19–22] which belong to a family broadly known as scorpionates,[2,23,24] and exploring their potential in coordination chemistry and metal-mediated processes. Fluorinated ligands are of interest because they act as weaker donors to metal ions and often endow different properties to metal complexes compared to their non-fluorinated, electron-rich equivalents.[25–34] They typically increase Lewis acidity at metal centers and enhance the volatility, oxidation resistance, and fluorocarbon solubility of their metal adducts. Additionally, they have been shown to improve the activity of certain metal-catalyzed reactions.

This paper describes structure and properties of thallium(I) and silver(I)–ethylene complexes supported by B-phenylated bis(pyrazolyl)borate ligands, $[Ph_2B(3\text{-}(CF_3)Pz)_2]^-$ (**1**) and $[Ph_2B(3\text{-}(SF_5)Pz)_2]^-$ (**2**), with CF_3 and SF_5 groups at the pyrazolyl ring 3-positions, and a B-phenylated bis(pyridyl)borate ligand $[Ph_2B(6\text{-}(CF_3)Py)_2]^-$ (**3**) with CF_3 groups at the pyridyl ring 6-positions (Fig. 1, Pz = pyrazolyl, Py = pyridyl). Fluorinated substituents on these ligands exhibit strong electron-withdrawing properties and shield the metal site by forming a chemically inert layer that protects parts of the periphery of the metal. The SF_5 group has been gaining more attention recently as a fluorinated substituent. However, unlike the CF_3 group,[34–39] it is still less widely used in chemistry,[40–46] and, in particular, in transition-metal chemistry.[22,47–54] The SF_5 group is often called the "super-trifluoromethyl group", and exhibits higher electronegativity than CF_3 (electronegativity parameters; χ = 3.65 [SF_5] *vs.* χ = 3.36 [CF_3]),[40,55] and bulkier than CF_3 with its size approaching that of *tert*-butyl group (van der Waals volumes; 61.4 Å^3 [SF_5] *vs.* 42.7 Å^3 [CF_3] *vs.* 76.4 Å^3 [^{t}Bu]).[56]

[a]*Department of Chemistry and Biochemistry, The University of Texas at Arlington, Arlington, Texas 76019, USA. E-mail: dias@uta.edu*
[b]*Enamine Ltd, Winston Churchill St 78, 02094 Kyiv, Ukraine*
[c]*Chemistry Department, Taras Shevchenko National University of Kyiv, Volodymyrska 64, 01601 Kyiv, Ukraine. E-mail: Pavel.Mykhailiuk@gmail.com*

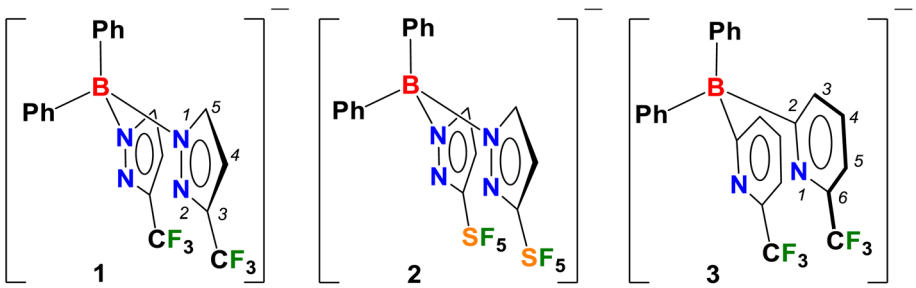

Fig. 1 B-phenylated bis(pyrazolyl)borate ligands $[Ph_2B(3\text{-}(CF_3)Pz)_2]^-$ (**1**), $[Ph_2B(3\text{-}(SF_5)Pz)_2]^-$ (**2**) and B-phenylated bis(pyridyl)borate ligand $[Ph_2B(6\text{-}(CF_3)Py)_2]^-$ (**3**), and the atom numbering schemes of pyrazolyl and pyridyl ring positions.

Silver(I) complexes with ethylene are of both fundamental and practical interest;[57] for example, silver plays a key role in ethylene epoxidation[58–60] and olefin separation.[61–63] Silver is also important in plant chemistry and horticulture because it has long been known to inhibit ethylene responses in plants.[64–66] Although extensive spectroscopic and computational research has been conducted on silver(I) ethylene adducts,[57,67,68] isolable silver(I) ethylene complexes are rare due to the weak σ-acceptor and poor π-donor properties of silver(I), which make them quite labile.[57,69–71] We also present structural data for thallium(I) complexes of **1–3**. They, in general, are good ligand transfer agents and can facilitate the separation and purification of scorpionate ligands from reaction mixtures.[23,72–77] Thallium complexes are also of interest for their NMR properties because Tl has two spin 1/2 isotopes, ^{203}Tl (29.5% natural abundance) and ^{205}Tl (70.5% natural abundance), leading to interesting spin–spin coupling between NMR active nuclei.[78–80]

Results and discussion

The syntheses of $[Ph_2B(3\text{-}(CF_3)Pz)_2]Tl$ (**4**) and $[Ph_2B(3\text{-}(SF_5)Pz)_2]Tl$ (**5**) were reported earlier,[22] but their molecular structures have not been reported. Here, we describe their X-ray crystal structures, highlight some interesting features, and present a higher-yield route (Scheme 1) to $[Ph_2B(3\text{-}(SF_5)Pz)_2]Tl$ (**5**).

Compound **5**, in the previous report, was synthesized by a solid-state reaction of $NaBPh_4$ with the corresponding pyrazole, $[3\text{-}(SF_5)Pz]H$, followed by the addition of TlOAc.[22] This method, however, proved somewhat inefficient by affording the desired thallium complex in only 36% overall yield. The modest outcome can be attributed to the relatively mild reactivity of $NaBPh_4$, which necessitated elevated reaction temperatures. Such conditions also required careful control to prevent the formation of by-products at higher temperatures (180 °C). To circumvent these limitations, a more reactive boron precursor, Ph_2BH_2Li,[81] was employed in the presence of $MeB(O^iPr)_2$ as a Lewis acid catalyst, which is expected to coordinate to, and decrease the pK_a of, the pyrazole and increase the rate of B–H bond protonolysis (Scheme 1).[82] This approach facilitated the formation of the lithium salt of the bis(pyrazolyl)borate, which, upon treatment with TlOAc, produced the thallium complex $[Ph_2B(3\text{-}(SF_5)Pz)_2]Tl$ (**5**) in 64% overall yield, representing a significant improvement over the original protocol. Molecular structures of $[Ph_2B(3\text{-}(SF_5)Pz)_2]Tl$ (**5**) as well as that of the $[Ph_2B(3\text{-}(CF_3)Pz)_2]Tl$ (**4**) have now been confirmed by single-crystal X-ray diffraction (Fig. 2).

The related bis(pyridyl)borate complex $[Ph_2B(6\text{-}(CF_3)Py)_2]Tl$ (**6**) was obtained by metathesis of its potassium salt, $[Ph_2B(6\text{-}(CF_3)Py)_2]K$[11] with TlOAc in 79% yield (Scheme 2). The crystal structure of **6** is shown in Fig. 3. All three thallium complexes of fluorinated scorpionates (**4–6**) described in this study were isolated as air- and moisture-stable off-white powders, free of coordinated solvent or water molecules. In general, these features of thallium complexes and their facile metathesis chemistry, compared to their alkali metal counterparts, make them promising precursors (ligand transfer agent) for the synthesis of various metal complexes. Selected bond lengths and angles of $[Ph_2B(3\text{-}(CF_3)Pz)_2]Tl$ (**4**), $[Ph_2B(3\text{-}(SF_5)Pz)_2]Tl$ (**5**), and $[Ph_2B(6\text{-}(CF_3)Py)_2]Tl$ (**6**) together with data for several related systems, are summarized in Table 1. The thallium complexes **4–6** adopt the expected κ^2-N,N coordination mode for the corresponding scorpionate. In compound **6**, there is a close separation between the *ipso*-carbon of the flanking phenyl group and thallium (2.833(3) Å). Thallium(I)-π-arene interactions are known and are typically found in thallium complexes or salts of weakly coordinating anions.[83–85] The arene-Tl separation in **6** falls within a region where weak but significant non-covalent interactions could occur. For comparison, it is within Bondi's Tl–C van der Waals contact distance of

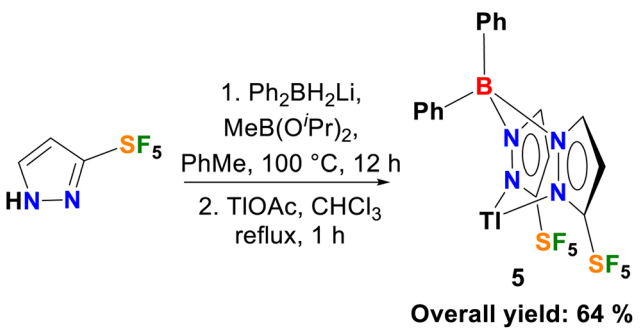

Scheme 1 Improved synthetic route to $[Ph_2B(3\text{-}(SF_5)Pz)_2]Tl$ (**5**).

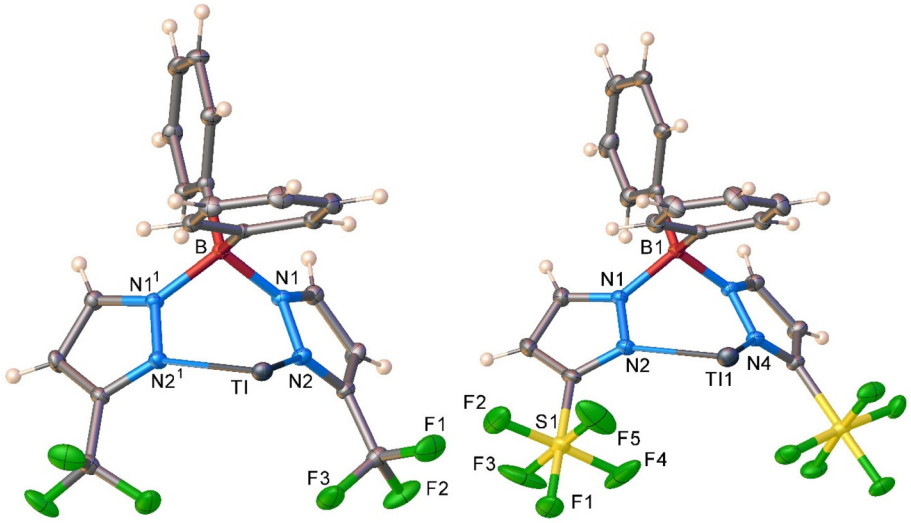

Fig. 2 Molecular structure of $[Ph_2B(3\text{-}(CF_3)Pz)_2]Tl$ (**4**, left) and $[Ph_2B(3\text{-}(SF_5)Pz)_2]Tl$ (**5**, right). Ellipsoids are shown at the 50% probability level.

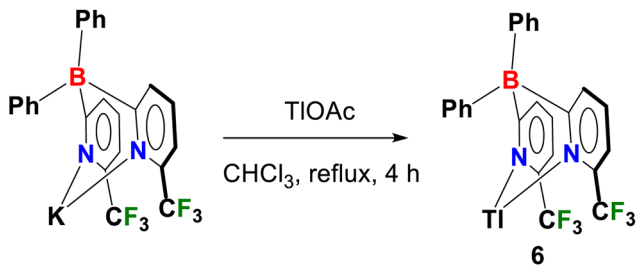

Scheme 2 Synthesis of $[Ph_2B(6\text{-}(CF_3)Py)_2]Tl$ (**6**).

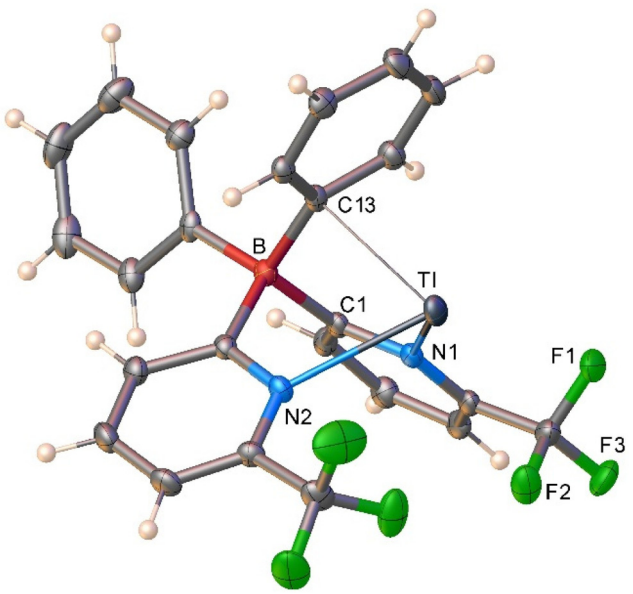

Fig. 3 Molecular structures of $[Ph_2B(6\text{-}(CF_3)Py)_2]Tl$ (**6**). Ellipsoids are shown at the 50% probability level.

3.66 Å,[86] but longer than the sum of the covalent radii of Tl and Csp^2 of 2.18 Å.[87]

A search in the Cambridge Structural Database (CSD)[88] resulted in 12 entities for structurally characterized thallium bis(pyrazolyl)borates, and none for thallium bis(pyridyl) borates, highlighting the limited structural data available for thallium complexes of these ligands. Analysis of the structural metrics reveals no clear trend in Tl–N bond distances of **6** compared to **4**, **5** and other bis(pyrazolyl)-based analogs, despite differences in the N-based heterocyclic donor arms (Table 1). These Tl–N bonds are longer than the sum of covalent radii (2.16 Å) but shorter than the van der Waals contact distance (3.51 Å).[89] More notable differences are observed in the N–Tl–N angles. Complex **4**, which has the least steric hindrance compared to complexes **5** and **6**, shows a relatively small N–Tl–N angle of 63.87°, yet it is clearly wider than that observed for $[H_2B(Pz)_2]Tl$ (55.5°), which is supported by the parent bis(pyrazolyl)borate ligand. This value N–Tl–N of **4** is smaller than those observed for complex **5** (67.60°) bearing the bulkier SF_5 groups at the same position, and complex **6** (68.86°), which is further enlarged due to the bulky nature of pyridyl-based ligand. Another notable difference is that the boat-shaped six-membered $Tl(NC)_2B$ core in **6** is deeper than the $Tl(NN)_2B$ cores in **4** and **5**, as evidenced by the shorter Tl···B separations in the former. There are no significant intermolecular interactions between thallium atoms in the solid state of complexes **4**–**6**. For instance, the closest intermolecular Tl···Tl separation in **4**, **5**, and **6** are 6.02, 6.27, and 6.02 Å, respectively, well above the sum of the Bondi's van der Waals radii for two thallium atoms (3.92 Å), indicating the absence of significant Tl···Tl interaction.[89–91]

An intriguing feature of thallium complexes supported by these fluorinated ligands is the observation of four-bond Tl–F coupling, likely a through-space interaction. Fluorinated bis(pyrazolyl/pyridyl)borate thallium complexes are limited; thus,

Table 1 Selected bond distances and angles of thallium complexes supported by bis(pyrazolyl)borate and bis(pyridyl)borate ligands

Compound	Tl–N (Å)	N–Tl–N (°)	Tl···B (Å)	Ref.
$[Ph_2B(3\text{-}(CF_3)Pz)_2]Tl$ (**4**)	2.688(2), 2.688(2)	63.87(9)	3.565	This work
$[Ph_2B(3\text{-}(SF_5)Pz)_2]Tl$ (**5**)	2.668(2) 2.686(2)	67.60(7)	3.563	This work
	2.682(2), 2.607(2)	*68.12(8)*	*3.571*	
$[H_2B(Pz)_2]Tl$	2.799(7), 2.814(8)	55.5(2)	3.34	92
$[H_2B(3,5\text{-}(CF_3)_2Pz)_2]Tl$	2.7243(19), 2.7243(19)	68.32(8)	3.364	93
$[H_2B(3,5\text{-}(^tBu)_2Pz)_2]Tl$	2.632(12), 2.645(12)	67.4(4)	3.176	94
$[H_2B(3\text{-}(^tBu),5\text{-}(^iPr)Pz)_2]Tl$	2.628(11), 2.664(10)	72.1(3)	3.179	94
$[H_2B(3\text{-}(^tBu),5\text{-}(Me)Pz)_2]Tl$	2.597(16), 2.59(3)	73.6(6)	3.118	94
$[H_2B(3\text{-}(Fc),5\text{-}(CF_3)Pz)_2]Tl$	2.578(5), 2.593(5)	76.54(15)	3.504	95
$[H_2B(3\text{-}(2\text{-pyrazinyl})Pz)_2]Tl$	2.644(4), 2.752(4)	71.28(11)	3.827	96
$[H_2B(3\text{-}(Trip)Pz)_2]Tl$	2.696(6), 2.705(6)	78.23(19)	3.313	97
$[Me(H)B(3\text{-}(Mes)Pz)_2]Tl$	2.636(5), 2.636(5)	79.1(2)	3.578	98
$[Ph_2B(6\text{-}(CF_3)Py)_2]Tl$ (**6**)	2.670(2), 2.675(2)	68.86(7)	3.459	This work

Abbreviations: Trip = 9-triptycyl, Mes = mesityl, Fc = ferrocenyl. Data for the second molecule in the asymmetric unit in italics.

the coupling constants of **4–6** are compared with related bis- and tris(pyrazolyl/pyridyl)borate systems (Table S1). Complex **5**, bearing both equatorial and axial fluorine atoms in the SF_5-groups, exhibits two distinct coupling constants ($^4J_{Tl-F}$ = 777 and 76 Hz; see Fig. S18).[22] The thallium complex **4** exhibits a smaller value of 576 Hz,[22] whereas complex **6** shows a remarkably larger $^4J_{Tl-F}$ of 1100 Hz. The coupling between thallium-203 and thallium-205 is not resolved in these signals, which is not unusual because their gyromagnetic ratios are similar, often making it impossible to distinguish the difference in ^{203}Tl and ^{205}Tl coupling constants.[78] The enhanced coupling in complex **6** can be attributed to the closer proximity of thallium to the CF_3 substituents at the 6-position of the pyridyl rings (with average $F_3C\cdots Tl$ separation of 3.58 Å) relative to the 3-position of pyrazolyl substituents (with average $F_3C\cdots Tl$ separation of 4.00 Å), allowing stronger through-space interaction with thallium. The Tl···C (of CF_3) separations in complex **6** are also shorter than those observed in tris- and bis(pyrazolyl)

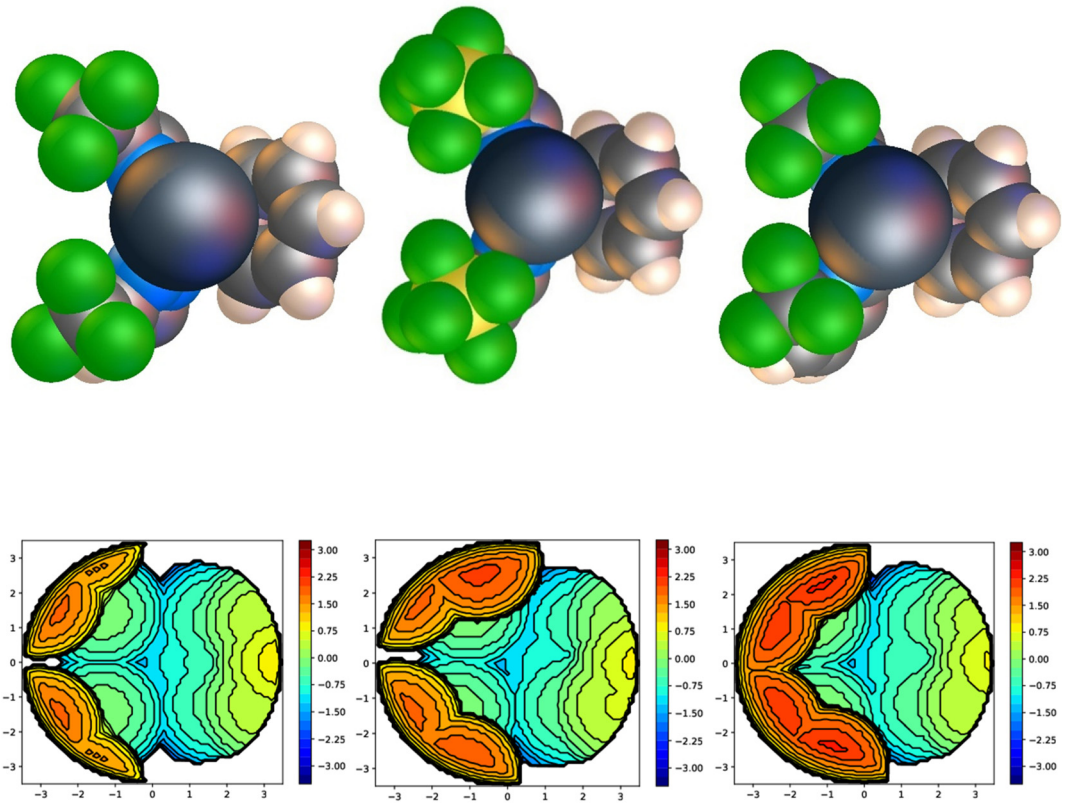

Fig. 4 Space-filling representations and steric maps of thallium complexes $[Ph_2B(3\text{-}(CF_3)Pz)_2]Tl$ (**4**, left) $[Ph_2B(3\text{-}(SF_5)Pz)_2]Tl$ (**5**, middle), and $[Ph_2B(6\text{-}(CF_3)Py)_2]Tl$ (**6**, right). The estimated $\%V_{Bur}$ values for complexes **4**, **5**, and **6** are 50.0%, 55.6% and 58.3%, respectively.

borate thallium complexes with CF_3-groups at the pyrazolyl ring 3-positions. However, we have recently reported a thallium complex of fluorinated tris(pyridyl)borate with relatively short $F_3C\cdots Tl$ separations (average 3.45 Å) with much larger $^4J_{Tl-F}$ (1208 Hz).[75] Further analysis indicates that there is a strong correlation between the $F_3C\cdots Tl$ separation and the Tl–F coupling constant (see Fig. S1), despite potential for complications in some cases.[78,79]

Space-filling models in Fig. 4 highlight the differing steric impacts of the B-phenylated and fluorinated ligand systems in complexes **4–6**. Yet another and more quantitative approach involves buried volume (%V_{Bur}) calculations and steric maps using the SambVca 2.1 web application,[99] in which the %V_{Bur} corresponds to the fraction of the volume of a sphere centered on the metal occupied by the coordinated ligand of focus, while the topographic steric map (Fig. 4) provides a graphical representation of the steric profile of a ligand using color-coded contour maps. For example, the %V_{Bur} values for complexes **4**, **5**, and **6** are 50.0%, 55.6% and 58.3%, respectively. Overall, the bis(pyridyl)borate framework in **6** affords the most protection around thallium, closely followed by the SF_5-substituted ligand in **5**, while the CF_3-substituted analog in **4** provides the least protection around thallium.

Although sodium, potassium and other alkali metal salts are more widely used as a transfer reagent due to their lower toxicity, thallium complexes sometimes serve as better scorpionate transfer agents due to their ease of purification and good solubility in non-polar solvents.[72,73,80] Scheme 3 illustrates the use of thallium complexes with AgOTf and under ethylene atmosphere to generate silver(I)–ethylene adducts, $[Ph_2B(3\text{-}(CF_3)Pz)_2]Ag(C_2H_4)$ (**7**), $[Ph_2B(3\text{-}(SF_5)Pz)_2]Ag(C_2H_4)$ (**8**), and $[Ph_2B(6\text{-}(CF_3)Py)_2]Ag(C_2H_4)$ (**9**). These are crystalline, colorless solids. Compounds **8** and **9** lose coordinated ethylene easily under reduced pressure. The X-ray crystal structures of **7–9** are presented in Fig. 5, with selected bond lengths and angles summarized in Table 2. They are three-coordinate, trigonal planar silver species featuring an η^2-bound C_2H_4. There is a close separation between the *ipso*-carbon of the flanking phenyl group of **9** and silver (2.6908(11) Å), which is within the Bondi's van der Waals contact separation of C and Ag (3.42 Å),[86,89] but this interaction does not seem to have a notable effect on silver, as evidenced by the sum of angles at silver being 360° (and the retention of trigonal planarity). For comparison, the sum of the covalent radii of silver and sp^2 carbon is 2.18 Å.[87] The scorpionate ligands in **7–9** coordinate to silver in a κ^2 fashion through the two nitrogen atoms from

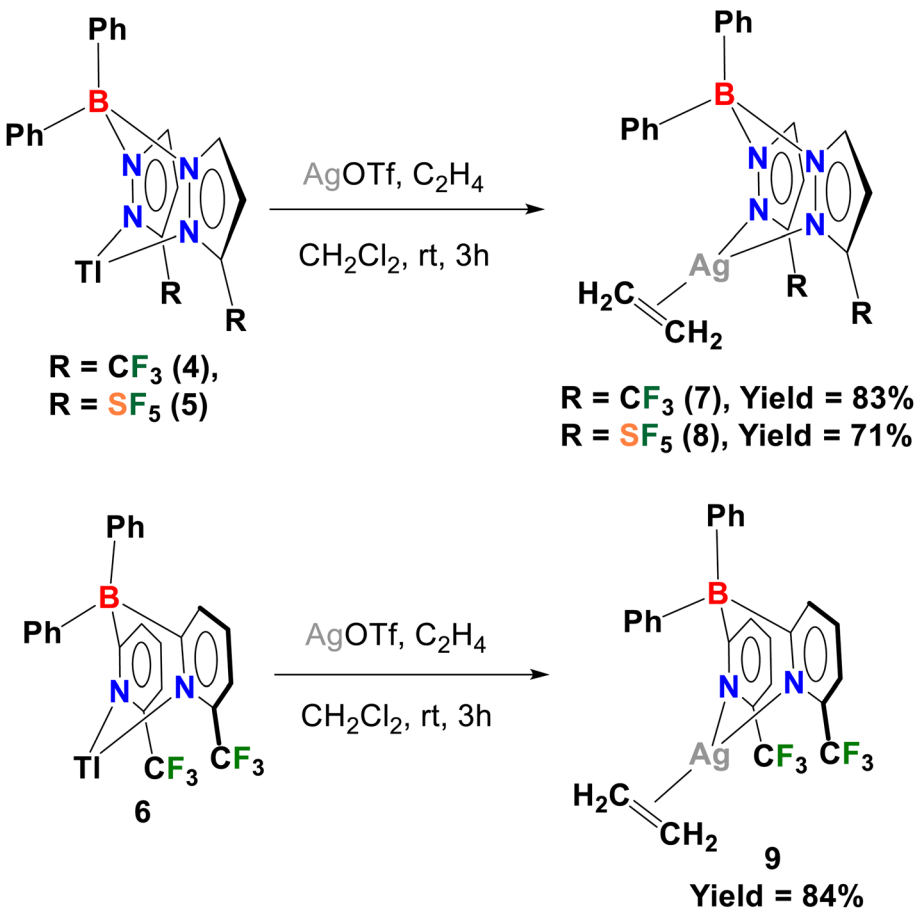

Scheme 3 Synthetic route to silver(I)-ethylene complexes $[Ph_2B(3\text{-}(CF_3)Pz)_2]Ag(C_2H_4)$ (**7**), $[Ph_2B(3\text{-}(SF_5)Pz)_2]Ag(C_2H_4)$ (**8**), and $[Ph_2B(6\text{-}(CF_3)Py)_2]Ag(C_2H_4)$ (**9**) supported by $[Ph_2B(3\text{-}(CF_3)Pz)_2]^-$, $[Ph_2B(3\text{-}(SF_5)Pz)_2]^-$, and $[Ph_2B(6\text{-}(CF_3)Py)_2]^-$ ligands.

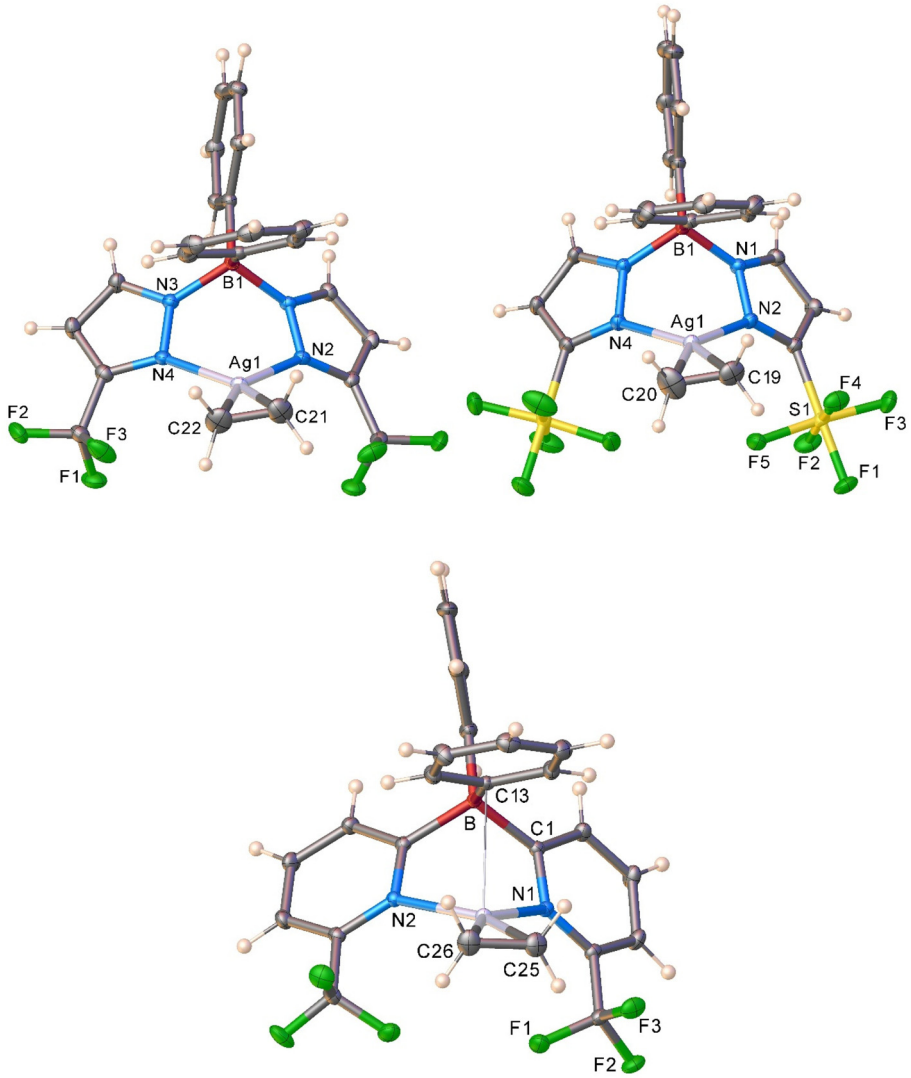

Fig. 5 Molecular structures of $[Ph_2B(3\text{-}(CF_3)Pz)_2]Ag(C_2H_4)$ (**7**, top-left), $[Ph_2B(3\text{-}(SF_5)Pz)_2]Ag(C_2H_4)$ (**8**, top-right), and $[Ph_2B(6\text{-}(CF_3)Py)_2]Ag(C_2H_4)$ (**9**, bottom). Ellipsoids are shown at the 50% probability level.

ligand arms, adopting the characteristic boat configuration. Most structural features are consistent across the three adducts; however, complexes **8** and **9** exhibit slightly longer Ag–C and Ag–N bond distances than those of complex **7**. These observed metrical parameters are attributable to the steric influence of the supporting ligands in **8** and **9**.

Percent buried volume ($\%V_{Bur}$)[99,100] of the scorpionate ligands in $[Ph_2B(3\text{-}(CF_3)Pz)_2]Ag(C_2H_4)$ (**7**), $[Ph_2B(3\text{-}(SF_5)Pz)_2]Ag(C_2H_4)$ (**8**), and $[Ph_2B(6\text{-}(CF_3)Py)_2]Ag(C_2H_4)$ (**9**), are 55.0%, 61.4%, and 64.5%, respectively, (Fig. 6). These values can be used to compare the steric bulkiness between the three supporting ligands, and indicate that $[Ph_2B(3\text{-}(CF_3)Pz)_2]^-$ provides the smallest, while $[Ph_2B(6\text{-}(CF_3)Py)_2]^-$ provides the highest steric protection to the silver–ethylene moiety in these molecules. This trend aligns with the values computed for the thallium complexes bearing the three ligands examined in this study (see above).

In the ^{1}H NMR spectrum at room temperature, the ethylene protons of **7** and **8** were observed at δ 4.67 and 4.73 ppm, respectively, while **9** shows its ethylene signal at δ 4.69 ppm. These protons likely experience the shielding cone of the B-phenyl group situated above the ethylene moiety, leading to larger than normal upfield shifts relative to the free C_2H_4 signal (δ 5.40 ppm).[71,102] For example, $[Me_2B(3\text{-}(CF_3)Py)_2]Ag(C_2H_4)$, which has a methyl group above the ethylene moiety, exhibits its ethylene proton resonance at a significantly downfield position, δ 5.42 ppm.[12] The ethylene carbons in **8** and **9** both appear as broad peaks at δ 103.9 ppm in their $^{13}C\{^1H\}$ NMR spectra, while in **7** the resonance is further upfield at δ 101.2 ppm. For comparison, the ethylene carbon peak of $[Me_2B(3\text{-}(CF_3)Py)_2]Ag(C_2H_4)$ appears in the same region at δ 102.8 ppm, while the resonance for free C_2H_4 was observed at δ 123.1 ppm.

Although ring current effects also could influence ^{13}C NMR shifts,[103] their through-space effects are generally smaller as

Table 2 Selected bond distances (Å) and angles (°) of silver–ethylene complexes **7–9** isolated in this work

Parameter	$[Ph_2B(3\text{-}(CF_3)Pz)_2]Ag(C_2H_4)$ (7)[c]	$[Ph_2B(3\text{-}(SF_5)Pz)_2]Ag(C_2H_4)$ (8)[d]	$[Ph_2B(6\text{-}(CF_3)Py)_2]Ag(C_2H_4)$ (9)
C═C	1.347(4) 1.352(5) 1.351(4)	1.339(3) 1.349(3)	1.346(2)
Ag–N	2.242(2), 2.266(2) 2.243(2), 2.243(2) 2.236(2), 2.272(2)	2.2828(13), 2.2883(13) 2.2827(13), 2.2707(13)	2.2767(10), 2.2732(10)
Ag–C	2.252(3), 2.262(3) 2.262(3), 2.241(3) 2.254(3), 2.266(3)	2.2697(18), 2.2733(19) 2.2724(19), 2.2689(19)	2.2710(13), 2.2701(13)
∠N–Ag–N	84.45(7) 85.75(7) 85.94(7)	79.01(5) 82.55(5)	84.46(4)
∠C–Ag–C	34.72(11) 34.93(12) 34.78(10)	34.28(8) 34.56(9)	34.49(5)
Ag···C(B)[a]	2.872 2.862 2.841	2.720 2.763	2.6908(11)
∑ at Ag[b]	360.22 360.11 360.87	359.98 360.00	359.61

[a] The Ag···C(B) is the *ipso*-carbon separation between the Ag and flanking phenyl group. [b] ∑ at Ag represents the sum of angles at silver involving two nitrogen atoms bonded to Ag and the centroid of the ethylene carbons. [c] Values for the three molecules in the asymmetric unit. [d] Values for the two molecules in the asymmetric unit.

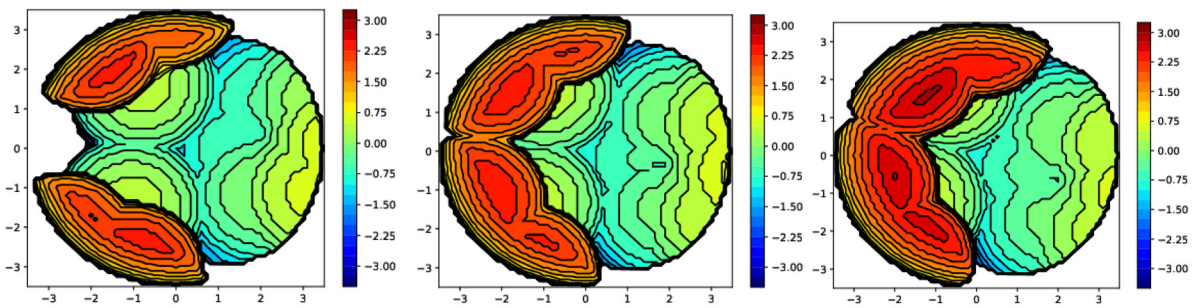

Fig. 6 Computed steric maps using SambVca 2.1[101] for supporting ligands in $[Ph_2B(3\text{-}(CF_3)Pz)_2]Ag(C_2H_4)$ (**7**, left), in $[Ph_2B(3\text{-}(SF_5)Pz)_2]Ag(C_2H_4)$ (**8**, middle), and $[Ph_2B(6\text{-}(CF_3)Py)_2]Ag(C_2H_4)$ (**9**, right), looking down the Ag···B axis.

they are further away from the flanking phenyl moiety. Thus, ^{13}C NMR shifts of the ethylene carbons serve as a useful probe of bonding interactions. The ethylene ^{13}C NMR resonance in the copper(I) complexes $[Ph_2B(3\text{-}(CF_3)Pz)_2]Cu(C_2H_4)$ and $[Ph_2B(3\text{-}(SF_5)Pz)_2]Cu(C_2H_4)$ have been observed at δ 82.7 and 86.4 ppm, respectively.[22] The upfield shifts of metal-bound ethylene ^{13}C resonances relative to free ethylene in these diamagnetic d^{10}-systems are commonly attributed to the increased metal-to-ethylene π back-donation effect.[57,71,104] The significantly higher upfield shifts in copper(I) complexes compared to their silver(I) counterparts **7** and **8** suggest that they exhibit greater π back-donation from the copper to ethylene. In fact, silver(I) in general forms the weakest interaction with ethylene among the group 11 family members.[105–107] Moreover, because the silver atom is larger than the copper atom,[87] replacing copper with silver in complexes bearing the same ligand and co-ligand results in smaller percent buried volumes. For instance, complexes **7** (55.0%) and **8** (61.4%) exhibit smaller buried volumes than their copper analogs $[Ph_2B(3\text{-}(CF_3)Pz)_2]Cu(C_2H_4)$ (59.5%)[108] and $[Ph_2B(3\text{-}(SF_5)Pz)_2]Cu(C_2H_4)$ (65.6%),[108] as the shorter Cu–ligand distances bring the ligand framework closer to the metal center (Fig. S2).

Silver–acetylene complexes are of considerable interest but remain rare, largely due to their instability toward decomposition.[109–111] Without suitable supporting ligands, these complexes are often too unstable to isolate. In our previous work, the $[Ph_2B(3\text{-}(CF_3)Pz)_2]^-$ (**1**) ligand enabled the successful isolation and structural characterization of a silver–acetylene complex, with ^1H and ^{13}C acetylene chemical shifts in $CDCl_3$ at δ 2.12 and 70.9 ppm.[111] Motivated by that result, we investigated the related $[Ph_2B(3\text{-}(SF_5)Pz)_2]^-$ (**2**) and $[Ph_2B(6\text{-}(CF_3)Py)_2]^-$ (**3**) ligands. The silver–acetylene complex $[Ph_2B(3\text{-}(SF_5)Pz)_2]Ag(C_2H_2)$ (**10**) was obtained by acetylene replacement of the corresponding ethylene adduct **8**. The NMR spectra of

10 in CD_2Cl_2 confirmed the presence of coordinated acetylene resonances, as evidenced by the δ 2.38 ppm peak in ^{1}H and the 68.6 ppm resonance in ^{13}C, both shifted from those of free C_2H_2 signals (δ 1.80, 71.9 ppm). However, it was unstable even at −20 °C, decomposing over time into an insoluble material, thereby precluding crystallographic analysis to date. An analogous attempt with $[Ph_2B(6\text{-}(CF_3)Py)_2]^-$ (**3**) resulted in rapid decomposition to a white solid and free ligand $[Ph_2B(6\text{-}(CF_3)Py)_2]H$ (**3**-*H*), as confirmed by ^{1}H NMR, indicating the instability of the pyridyl-based system under such reaction conditions.

Finally, the catalytic behavior of CF_3-group bearing bis(pyrazolyl)borate $[Ph_2B(3\text{-}(CF_3)Pz)_2]Ag(C_2H_4)$ (**7**) and bis(pyridyl)borate $[Ph_2B(6\text{-}(CF_3)Py)_2]Ag(C_2H_4)$ (**9**) complexes was examined in the context of alkane C–H functionalization through carbene transfer reactions from carbene precursor, ethyl diazoacetate, N_2CHCO_2Et (EDA). Previous studies from our group and Pérez's group have shown that silver complexes supported by weakly donating tris(pyrazolyl)borate ligands can enhance the electrophilicity of the metal center, thereby improving catalytic efficiency.[57,112–119] Compared to copper(I), silver(I) can more effectively activate less reactive C–H bonds, such as those at primary C–H sites.[114] Moreover, silver-based catalysts can often perform these reactions without requiring the slow addition of carbene precursors, a procedure commonly necessary for copper(I) systems to suppress the formation of undesired byproducts. Overall, the catalytic data reveal that the nature of the supporting ligand significantly influences both the activity and regioselectivity of the carbene insertion reaction. Catalysts **7** and **8**, which contain more Lewis acidic silver centers, afford higher yields of C–H insertion products than catalyst **9**, which features the more electron-donating pyridyl-based ligand (see Table 3 and Tables S8, S9 for more details). The greater electrophilicity of the metal center in **7** and **8**[11] likely facilitates the formation of the silver–carbene intermediate and promotes more efficient C–H bond insertion. In contrast, the increased electron density at the metal center in **9** may reduce its carbene electrophilicity, thereby lowering overall reactivity towards C–H moieties. In addition to these electronic effects, steric factors govern regioselectivity. Complex **9**, supported by the bulkier pyridyl-based ligand,

Table 3 Regioselectivity[a] and yields of C–H functionalization *via* carbene insertion (from ethyl diazoacetate, EDA) with CF_3-decorated bis(pyrazolyl/pyridyl)borate Ag catalysts $[Ph_2B(3\text{-}(CF_3)Pz)_2]Ag(C_2H_4)$ (**7**), $[Ph_2B(3\text{-}(SF_5)Pz)_2]Ag(C_2H_4)$ (**8**), and $[Ph_2B(6\text{-}(CF_3)Py)_2]Ag(C_2H_4)$ (**9**), and an illustration of carbene insertion products from EDA on 2-methylbutane substrate (entries 7–9)

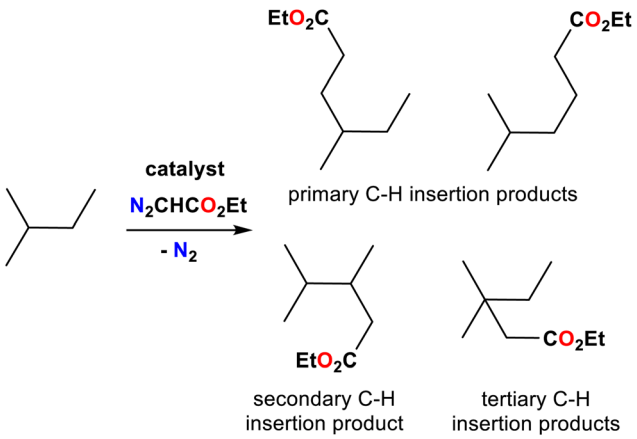

Entry	Cat.	Substrate	Primary sites	Secondary sites	Tertiary sites	Yields (%)
1	**7**		—	1	—	90
2	**8**		—	1	—	90
3	**9**		—	1	—	61
4	**7**		1	2.88	—	93
5	**8**		1	2.18	—	89
6	**9**		1	1.94	—	56
7	**7**		1	—	7.71	96
8	**8**		1	—	5.47	89
9	**9**		1	—	3.50	38
10	**7**		1	2.92	6.32	87
11	**8**		1	3.53	6.07	86
12	**9**		1	2.10	3.60	56

[a] Values normalized for the relative number of C–H bonds each type, calculated from the observed carbene insertion product ratios and the number of C–H bonds of each type.

favors functionalization at primary C–H sites. This observation suggests that the increased steric congestion around the metal center limits the approach of secondary or tertiary C–H bonds, which are more hindered, and agrees with previous observations.[118,120] These results illustrate that both electronic and steric features of the ligand framework can be strategically modulated to fine-tune the reactivity and selectivity of silver(I) carbene-transfer catalysts. Although the effectiveness achieved with some of these bis(pyrazolyl/pyridyl)borate-supported systems – especially the more electron-rich bis(pyridyl)borate-silver system – does not surpass that of more electrophilic and sterically encumbered tris(pyrazolyl)borate catalysts such as $[HB(3,5\text{-}(CF_3)_2Pz)_3]Ag(C_2H_4)$[113] or $[HB(3,4,5\text{-}(Br)_3Pz)_3]Ag(THF)$,[120] the data underscore the importance of balancing metal electrophilicity and ligand steric demand in optimizing C–H bond functionalization processes.

Conclusions

In summary, fluorinated and B-phenylated bis(pyrazolyl)borate and bis(pyridyl)borate ligands have been synthesized and evaluated as sterically and electronically tunable scorpionate platforms for stabilizing thallium(I) and silver(I) complexes, including rare isolable silver–ethylene adducts. The ligands $[Ph_2B(3\text{-}(CF_3)Pz)_2]^-$ (**1**), $[Ph_2B(3\text{-}(SF_5)Pz)_2]^-$ (**2**) and $[Ph_2B(6\text{-}(CF_3)Py)_2]^-$ (**3**) incorporate strongly electron-withdrawing CF_3 or SF_5 substituents that introduce pronounced steric shielding; notably, SF_5 substituents provide both greater electronegativity and steric bulk relative to CF_3, and the bis(pyridyl)borate framework imparts still greater steric congestion around the metal center relative to bis(pyrazolyl)borates. Thallium(I) complexes exhibit characteristic κ^2-N,N binding of the scorpionate ligand, along with measurable long-range thallium-203/205-fluorine-19 coupling that correlates directly with through-space Tl···F separations. These thallium complexes serve as efficient ligand-transfer reagents to silver, providing access to silver(I) ethylene complexes, in which the ^{1}H and ^{13}C NMR data reveal ethylene resonances shifted upfield relative to those of free C_2H_4, and their X-ray crystal structures show trigonal-planar silver sites. Comparative ^{13}C NMR data indicate significantly weaker π-backbonding in Ag–ethylene compared to analogous Cu complexes, consistent with established trends in group 11 olefin binding. The use of silver catalysts with varying electronic and steric ligands strongly influences C–H functionalization of alkanes *via* carbene insertion. More electrophilic metal centers enhance reactivity and yields, while bulkier or more electron-rich ligands favor functionalization at less hindered primary sites. Overall, the work demonstrates how fluorinated substituents and heterocyclic donor arms in scorpionate ligands govern metal–ligand geometry, Tl–F coupling, steric environment, and the stability of labile silver π-complexes, and provides a versatile platform for developing catalysts for selective C–H functionalization.

Experimental section

General information

All preparations and manipulations were carried out under an atmosphere of purified nitrogen using standard Schlenk techniques or in a vacuum atmosphere single-station dry box equipped with a −25 °C refrigerator. NMR solvents were purchased from Cambridge Isotopes Laboratories and used as received. Dichloromethane, toluene, and hexane were dried by passing HPLC-grade solvent through a solvent purification system (SPS, Innovative Technologies Inc.) and stored in Straus flasks. NMR spectra were recorded at 25 °C on a JEOL Eclipse 500 (^{1}H, 500 MHz; ^{13}C, 126 MHz; and ^{19}F, 471 MHz), JEOL Eclipse 400 spectrometer (^{1}H, 400 MHz; ^{13}C, 100 MHz, ^{19}F, 376 MHz), or JEOL Eclipse 300 (^{1}H, 300 MHz; ^{13}C, 75 MHz; and ^{19}F, 273 MHz). ^{1}H and $^{13}C\{^1H\}$ NMR spectra are referenced to the solvent peak (^{1}H, $CDCl_3$ δ 7.26; ^{13}C, $CDCl_3$ δ 77.16, CD_2Cl_2 δ 54.00). ^{19}F NMR values were referenced to external $CFCl_3$. ^{1}H, $^{13}C\{^1H\}$, and ^{19}F NMR chemical shifts are reported in ppm and coupling constants (J) are reported in hertz (Hz). Abbreviations used for signal assignments: Py = pyridyl, Ph = phenyl, s = singlet, d = doublet, t = triplet, q = quartet, pent = pentet, m = multiplet, br = broad, brs = broad singlet. Elemental analyses were performed using a PerkinElmer Model 2400 CHN analyzer. IR spectra were collected at room temperature on a Shimadzu IR Prestige-21 FTIR equipped with an ATR attachment using pure liquid or solid samples, with a resolution of 2 cm^{-1}. Raman data were collected on a Thermo Scientific DXR3 Raman microscope using a 633 nm HeNe laser, with pure solid materials placed on a glass slide. $[Ph_2B(6\text{-}(CF_3)Py)_2]K$,[11] Ph_2BH_2Li,[81] and $MeB(O^iPr)_2$ [121] were synthesized as previously reported. Compound $[Ph_2B(3\text{-}(CF_3)Pz)_2]Tl$[22] was prepared by a modified process as noted below. All other reactants and reagents were purchased from commercial sources or obtained as noted below.

Synthetic procedures

Warning: Thallium salts are toxic; therefore, these compounds should be handled with proper precautions.[122] Care must be taken to prevent exposure through inhalation, accidental ingestion *via* contaminated hands or gloves, or skin contact. Waste products should be disposed of properly. Silver in combination with acetylene gas can lead to potentially explosive materials and should be prepared in small quantities and handled with appropriate precautions. While no difficulties were encountered with the complexes reported herein, caution should be exercised. Due care must also be taken when working with acetylene gas and handling acetylene tanks. It is known to produce explosive combinations with oxygen.

$[Ph_2B(3\text{-}(SF_5)Pz)_2]Tl$ (5). Ph_2BH_2Li (90.2 mg, 0.52 mmol) was weighed and transferred to a 50 mL Schlenk flask inside the glove box. The compound was taken outside and dissolved in 2 mL dry toluene. A solution of 5-(pentafluoro-λ^6-sulfanyl)-1*H*-pyrazole (200.00 mg, 1.03 mmol) in 3 mL dry toluene was added dropwise to the Ph_2BH_2Li solution under nitrogen atmosphere at room temperature. $MeB(O^iPr)_2$ (14.8 mg, 0.1 mmol) was added to the reaction and was heated at 100 °C

under nitrogen overnight. The reaction was cooled to room temperature and cannula filtered through a Celite-packed frit to a 50 mL Schlenk flask. The reaction flask was rinsed with 2 mL toluene and filtered. The solvent was evaporated to get $[Ph_2B(3\text{-}(SF_5)Pz)_2]Li$ as a white powder. The lithium salt was dissolved in 10 mL dry chloroform. Tl(OAc) (164.40 mg, 0.62 mmol) was added to the solution, and the resulting mixture was refluxed for 1 h. The reaction was cooled to room temperature and filtered through a Celite-packed frit. The solvent was evaporated to get the product as a white powder. X-ray quality crystals of $[Ph_2B(3\text{-}(SF_5)Pz)_2]Tl$ were obtained in chloroform at room temperature by slow evaporation in 64% overall yield. The NMR data agree with the published values.[22]

$[Ph_2B(6\text{-}(CF_3)Py)_2]Tl$ (6). To a mixture of $[Ph_2B(6\text{-}(CF_3)Py)_2]K$ (200 mg, 0.402 mmol) and TlOAc (159 mg, 0.604 mmol) in a 50 mL Schlenk flask, 25 mL of anhydrous chloroform was added, and the resulting mixture was then refluxed for 4 hours. After cooling to room temperature, the reaction mixture was cannula-filtered through a Celite-packed frit to remove KOAc and excess TlOAc. The solvent was then removed under reduced pressure, resulting in an off-white solid. Single crystals of $[Ph_2B(6\text{-}(CF_3)Py)_2]Tl$, suitable for X-ray analysis, were grown by slow evaporation of its chloroform solution at room temperature. Yield: 210 mg (79%). ^{1}H NMR (500 MHz, $CDCl_3$): δ (ppm) 8.10 (d, J = 7.9 Hz, 2H, Py), 7.61 (t, J = 7.8 Hz, 2H, Py), 7.44 (d, J = 7.5 Hz, 2H, Py), 7.33 (t, J = 7.4 Hz, 4H, Ph), 7.29–7.19 (m, 5H, Ph). $^{13}C\{^1H\}$ NMR (126 MHz, $CDCl_3$): δ (ppm) 187.4 (q, $^1J_{B-C}$ = 52.8 Hz, Py), 159.0 (br, Ph), 145.5 (q, $^2J_{F-C}$ = 33.6 Hz, *C*-CF_3), 136.4 (Ph/Py), 135.2 (Ph/Py), 134.6 (Ph/Py), 128.6 (Ph/Py), 125.6 (Ph/Py), 123.0 (q, $^1J_{F-C}$ = 275.9 Hz, *C*F_3), 116.7 (Py). ^{19}F NMR (471 MHz, $CDCl_3$): δ (ppm) −64.92 (d, $^4J_{Tl-F}$ = 1100.4 Hz). HR-MS [ESI, positive ion mode ESI-TOF]: m/z for $C_{24}H_{16}B_1F_6N_2Tl_1$ $[M + H]^+$ calcd 663.1133, found 663.1046.

$[Ph_2B(3\text{-}(CF_3)Pz)_2]Ag(C_2H_4)$ (7). $[Ph_2B(3\text{-}(CF_3)Pz)_2]Tl$ (0.30 g, 0.47 mmol) and AgOTf (0.13 g, 0.47 mmol) were taken in a 50 mL Schlenk flask and 20 mL ethylene-saturated CH_2Cl_2 was added into it. The reaction mixture was stirred for 3 h at room temperature under an ethylene atmosphere. The reaction mixture was cannula filtered through a Celite-packed frit. The filtrate was concentrated under reduced pressure to about 3 mL, then further concentrated with a continuous flow of ethylene until close to saturation, and stored at −20 °C under a blanket of ethylene to obtain X-ray-quality colorless crystals of $[Ph_2B(3\text{-}(CF_3)Pz)_2]Ag(C_2H_4)$. Yield: 83%. Anal. calc. $C_{22}H_{18}AgBCuF_6N_4$: C, 46.27; H, 3.18%; N, 9.81%. Found: C, 45.86%; H, 2.93%; N, 9.64%. ^{1}H NMR ($CDCl_3$): δ (ppm) 7.72 (s, 2H, Pz), 7.28–7.27 (m, 6H, Ph), 6.90 (br, 4H, Ph), 6.50 (br, 2H, Pz), 4.67 (s, 4H, C_2H_4). $^{13}C\{^1H\}$ NMR ($CDCl_3$): δ (ppm) 142.8 (q, $^2J_{F-C}$ = 37.2 Hz, *C*-CF_3), 138.4 (Ph), 134.7 (Pz), 127.5 (Ph), 127.1 (Ph), 121.4 (q, $^1J_{C-F}$ = 268.7 Hz, *C*F_3), 102.8 (Pz), 101.2 (C═C). ^{19}F NMR ($CDCl_3$): δ (ppm) −61.5 (s).

$[Ph_2B(3\text{-}(SF_5)Pz)_2]Ag(C_2H_4)$ (8). $[Ph_2B(3\text{-}(SF_5)Pz)_2]Tl$ (0.10 g, 0.13 mmol) and AgOTf (0.04 g, 0.13 mmol) were taken in a 50 mL Schlenk flask and 10 mL ethylene-saturated CH_2Cl_2 was added into it. The reaction mixture was stirred for 3 h at room temperature under an ethylene atmosphere. Ethylene gas was bubbled three times during the reaction (30 seconds each time). The reaction mixture was cannula-filtered through a Celite-packed frit using nitrogen gas. The filtrate was concentrated under reduced pressure to about 3 mL, then further concentrated with a continuous flow of ethylene until close to saturation, and stored at −20 °C under a blanket of ethylene to obtain X-ray-quality colorless crystals of $[Ph_2B(3\text{-}(SF_5)Pz)_2]Ag(C_2H_4)$. Yield: 71%. M.p.: 215–218 °C (decomposition). ^{1}H NMR ($CDCl_3$): δ (ppm) 7.69 (s, 2H, Pz), 7.31–7.30 (m, 6H, Ph), 6.94 (br, 4H, Ph), 6.49 (d, J = 2.3 Hz, 2H, Pz), 4.73 (s, 4H, C_2H_4). $^{13}C\{^1H\}$ NMR ($CDCl_3$): δ (ppm) 160.1 (q, $^1J_{C-B}$ = 26.4 Hz, B-Ph), 137.7 (Ph), 134.9 (Pz), 132.8 (Pz), 127.7 (Ph), 127.5 (Ph), 103.9 (br, C═C), 102.6 (Pz). ^{19}F NMR ($CDCl_3$): δ (ppm) 81.70 (pent, $^2J_{F-F}$ = 154.8 Hz, 2F), 64.53 (d, $^2J_{F-F}$ = 154.8 Hz, 8F).

$[Ph_2B(6\text{-}(CF_3)Py)_2]Ag(C_2H_4)$ (9). To a mixture of $[Ph_2B(6\text{-}(CF_3)Py)_2]Tl$ (100 mg, 0.151 mmol) and AgOTf (43 mg, 0.166 mmol) in a 50 mL Schlenk flask covered with aluminum foil, was added anhydrous dichloromethane (20 mL) and then bubbled with ethylene, kept stirring for 3 h. The reaction mixture was then cannula filtered through a Celite-packed frit. The solvent was then removed under reduced pressure. The compound was recrystallized from an ethylene-saturated dichloromethane/hexane solution at 4 °C to obtain colorless X-ray quality single crystals of $[Ph_2B(6\text{-}(CF_3)Py)_2]Ag(C_2H_4)$. Yield: 75 mg (84%). Anal. calc. $C_{26}H_{20}BAgF_6N_2{\cdot}0.4CH_2Cl_2$: C, 50.56; H, 3.34; N, 4.47%. Found: C, 50.87; H, 3.12; N, 4.41. ^{1}H NMR (500 MHz, $CDCl_3$): δ (ppm) 8.10 (d, J = 7.4 Hz, 2H, Py), 7.61 (t, J = 7.7 Hz, 2H, Py), 7.42 (d, J = 8.0 Hz, 2H, Py), 7.29–7.03 (brs, 10H, Ph), 4.69 (s, 4H, C_2H_4). $^{13}C\{^1H\}$ (126 MHz, $CDCl_3$): δ (ppm) 187.5 (q, $^1J_{B-C}$ = 54.6 Hz, B-Py), 154.4 (q, $^1J_{B-C}$ = 47.7 Hz, B-Ph), 146.0 (q, $^2J_{C-F}$ = 32.42 Hz, Py), 136.3 (Py), 135.3 (Py), 133.8 (Ph), 127.3 (Ph), 124.3 (Ph), 122.1 (q, $^1J_{C-F}$ = 274 Hz, CF_3), 116.5 (Py), 103.9 (C_2H_4). ^{19}F NMR (471 MHz, $CDCl_3$): δ (ppm) −67.41 (s).

$[Ph_2B(3\text{-}(SF_5)Pz)_2]Ag(C_2H_2)$ (10). $[Ph_2B(3\text{-}(SF_5)Pz)_2]Ag(C_2H_4)$ (0.10 g, 0.17 mmol) and was dissolved in 4 mL CH_2Cl_2 in a 50 mL Schlenk flask and purified acetylene was bubbled into the flask for 2 minutes. The compound was dried under a continuous flow of acetylene to get the product as a white powder. Attempts to obtain single crystals of the complex were unsuccessful. Yield: 79%. ^{1}H NMR (CD_2Cl_2): δ (ppm) 7.83 (br, 2H), 7.66–7.46 (m, 4H), 7.34–7.28 (m, 6H), 6.70 (d, J = 2 Hz, 2H, Pz), 2.38 (s, 2H, C_2H_2). $^{13}C\{^1H\}$ NMR (CD_2Cl_2): δ (ppm) 160.5 (q, $^1J_{C-B}$ = 21.4 Hz, B-Ph), 138.2 (Pz), 135.2 (Ph), 128.1 (Ph), 127.6 (Ph), 103.0 (Pz), 68.6 (C≡C). ^{19}F NMR (CD_2Cl_2): δ (ppm) 81.5 (pent, $^2J_{F-F}$ = 154.8 Hz, 2F), 64.2 (d, $^2J_{F-F}$ = 154.8 Hz, 8F). Note: the compound readily loses acetylene under vacuum. The compound is not stable even at −20 °C for a long time. A white insoluble precipitate appears in methylene chloride. The complex decomposes in NMR solvent.

X-ray structure determinations

A suitable crystal covered with a layer of hydrocarbon/Paratone-N oil was selected and mounted on a Cryo-loop, and immediately placed in the low temperature nitrogen stream. The X-ray intensity data were measured at 100(2) K (unless otherwise noted) on a Bruker Smart ApexII or Bruker D8 Quest

equipped with an Oxford Cryosystems 700 series cooler, a graphite monochromator, and a Mo Kα fine-focus sealed tube (λ = 0.71073 Å). Intensity data were processed, and absorption corrections were applied using the Bruker Apex program suite. Initial atomic positions were located by SHELXT,[123] and the structures of the compounds were refined by the least-squares method using SHELXL[124] within Olex2 GUI.[125] Compounds $[Ph_2B(3\text{-}(SF_5)Pz)_2]Tl$ (**5**) and $[Ph_2B(3\text{-}(SF_5)Pz)_2]Ag(C_2H_4)$ (**8**) and $[Ph_2B(3\text{-}(CF_3)Pz)_2]Ag(C_2H_4)$ (**7**) crystallize with two, two, and three chemically identical but crystallographically different molecules of each type in the asymmetric unit, respectively. Fluorine atoms in one of the CF_3 groups of $[Ph_2B(3\text{-}(CF_3)Pz)_2]Ag(C_2H_4)$ (**7**), and the equatorial fluorine atoms of one of the SF_5 groups of $[Ph_2B(3\text{-}(SF_5)Pz)_2]Ag(C_2H_4)$ show positional disorder, but it was modeled satisfactorily. All the non-hydrogen atoms in **4–9** were refined anisotropically. Hydrogen atoms of the ethylene carbons of $[Ph_2B(6\text{-}(CF_3)Py)_2]Ag(C_2H_4)$ (**9**) were located on difference maps, included and refined freely. The remaining hydrogen atoms of **9** and those of **4–8** were included at calculated positions and refined using appropriate riding models. X-ray structural figures were generated using Olex2.

Conflicts of interest

There are no conflicts to declare.

Data availability

Supplementary information (SI): NMR spectroscopic data, steric volumes, additional figures, summaries of data collection and refinement, catalysis, and references. See DOI: https://doi.org/10.1039/d5dt02782a.

CCDC 2498963–2498968 and 2504337 contain the supplementary crystallographic data for this paper.[126a–g]

Acknowledgements

This research was supported in part by the USDA REE, Agricultural Research Services (58-2040-3-017), and a grant from the American Floral Endowment, an industry-funded nonprofit dedicated to sustaining and advancing floriculture research. We also acknowledge the support from The University of Texas at Arlington.

References

1 S. Trofimenko, *J. Am. Chem. Soc.*, 1966, **88**, 1842–1844.
2 S. Trofimenko, *Chem. Rev.*, 1993, **93**, 943–980.
3 C. Pettinari and C. Santini, Polypyrazolylborate and scorpionate ligands, in *Comprehensive Coordination Chemistry II: From Biology to Nanotechnology*, ed. J. A. McCleverty and T. J. Meyer, Elsevier, Amsterdam, 2003, vol. 1, pp. 159–210.
4 T. G. Hodgkins, *Inorg. Chem.*, 1993, **32**, 6115–6116.
5 T. G. Hodgkins and D. R. Powell, *Inorg. Chem.*, 1996, **35**, 2140–2148.
6 B. L. Conley and T. J. Williams, *J. Am. Chem. Soc.*, 2010, **132**, 1764–1765.
7 B. L. Conley, D. Guess and T. J. Williams, *J. Am. Chem. Soc.*, 2011, **133**, 14212–14215.
8 Z. Lu, B. Malinoski, A. V. Flores, B. L. Conley, D. Guess and T. J. Williams, *Catalysts*, 2012, **2**, 412–421.
9 J. A. Celaje, M. K. Pennington-Boggio, R. W. Flaig, M. G. Richmond and T. J. Williams, *Organometallics*, 2014, **33**, 2019–2026.
10 M. K. Pennington-Boggio, B. L. Conley, M. G. Richmond and T. J. Williams, *Polyhedron*, 2014, **84**, 24–31.
11 M. Vanga, A. Noonikara-Poyil, J. Wu and H. V. R. Dias, *Organometallics*, 2022, **41**, 1249–1260.
12 B. T. Watson, M. Vanga, A. Noonikara-Poyil, A. Munoz-Castro and H. V. R. Dias, *Inorg. Chem.*, 2023, **62**, 1636–1648.
13 S. Pal, P. Y. Zavalij and A. N. Vedernikov, *Organometallics*, 2015, **34**, 5183–5190.
14 E. Khaskin, P. Y. Zavalij and A. N. Vedernikov, *J. Am. Chem. Soc.*, 2006, **128**, 13054–13055.
15 V. A. Krylova, P. I. Djurovich, B. L. Conley, R. Haiges, M. T. Whited, T. J. Williams and M. E. Thompson, *Chem. Commun.*, 2014, **50**, 7176–7179.
16 S. Pal and A. N. Vedernikov, *Dalton Trans.*, 2012, **41**, 8116–8122.
17 A. Gogoi, P. Singh, S. Pal and M. Dixit, *Inorg. Chem.*, 2022, **61**, 10283–10293.
18 S. Stipurin and T. Strassner, *Organometallics*, 2024, **43**, 1726–1735.
19 H. V. R. Dias and J. D. Gorden, *Inorg. Chem.*, 1996, **35**, 318–324.
20 T. T. Ponduru, Z. Sun, T. R. Cundari and H. V. R. Dias, *ChemCatChem*, 2019, **11**, 4966–4973.
21 A. Noonikara-Poyil, S. G. Ridlen and H. V. R. Dias, *Inorg. Chem.*, 2020, **59**, 17860–17865.
22 A. Noonikara-Poyil, A. Munoz-Castro, A. Boretskyi, P. K. Mykhailiuk and H. V. R. Dias, *Chem. Sci.*, 2021, **12**, 14618–14623.
23 C. Pettinari, *Scorpionates II: Chelating Borate Ligands*, World Scientific, 2008.
24 P. J. Fischer, in *Comprehensive Coordination Chemistry III*, ed. E. C. Constable, G. Parkin and L. Que Jr, Elsevier, Oxford, 2021, pp. 428–504, DOI: 10.1016/B978-0-08-102688-5.00072-6.
25 L. H. Doerrer and H. V. R. Dias, *Dalton Trans.*, 2023, **52**, 7770–7771.
26 S. M. Park, M. Wei, J. Xu, H. R. Atapattu, F. T. Eickemeyer, K. Darabi, L. Grater, Y. Yang, C. Liu, S. Teale, B. Chen, H. Chen, T. Wang, L. Zeng, A. Maxwell, Z. Wang, K. R. Rao, Z. Cai, S. M. Zakeeruddin, J. T. Pham, C. M. Risko, A. Amassian, M. G. Kanatzidis, K. R. Graham, M. Grätzel and E. H. Sargent, *Science*, 2023, **381**, 209–215.
27 J. C. Páez-Franco, M. R. Zermeño-Ortega, C. M. de la O-Contreras, D. Canseco-González, J. R. Parra-Unda,

A. Avila-Sorrosa, R. G. Enríquez, J. M. Germán-Acacio and D. Morales-Morales, *Pharmaceutics*, 2022, **14**, 402.
28 R. Pedrazzani, S. Kiriakidi, M. Monari, I. Lazzarini, G. Bertuzzi, C. S. López and M. Bandini, *ACS Catal.*, 2024, **14**, 6128–6136.
29 W. Chen, L. Xu, Y. Hu, A. M. Banet-Osuna and J. Xiao, *Tetrahedron*, 2002, **58**, 3889–3899.
30 S. Mishra and S. Daniele, *Chem. Rev.*, 2015, **115**, 8379–8448.
31 A. C. Sather, H. G. Lee, V. Y. De La Rosa, Y. Yang, P. Müller and S. L. Buchwald, *J. Am. Chem. Soc.*, 2015, **137**, 13433–13438.
32 S. Dehnen, L. L. Schafer, T. Lectka and A. Togni, *Organometallics*, 2021, **40**, 3858–3864.
33 V. I. Saloutin, Y. O. Edilova, Y. S. Kudyakova, Y. V. Burgart and D. N. Bazhin, *Molecules*, 2022, **27**, 7894.
34 M. A. García-Monforte, S. Martínez-Salvador and B. Menjón, *Eur. J. Inorg. Chem.*, 2012, **2012**, 4945–4966.
35 P. K. Mykhailiuk, *Chem. Rev.*, 2021, **121**, 1670–1715.
36 O. A. Tomashenko and V. V. Grushin, *Chem. Rev.*, 2011, **111**, 4475–4521.
37 C. Alonso, E. Martínez de Marigorta, G. Rubiales and F. Palacios, *Chem. Rev.*, 2015, **115**, 1847–1935.
38 T. Furuya, A. S. Kamlet and T. Ritter, *Nature*, 2011, **473**, 470–477.
39 H. Jia, A. P. Häring, F. Berger, L. Zhang and T. Ritter, *J. Am. Chem. Soc.*, 2021, **143**, 7623–7628.
40 P. R. Savoie and J. T. Welch, *Chem. Rev.*, 2015, **115**, 1130–1190.
41 Y. Yang, L. Han, L. Brettnacher, L. Canavero and A. Tlili, *Chem. Rev.*, 2025, **125**, 8426–8476.
42 J. M. W. Chan, *J. Mater. Chem. C*, 2019, **7**, 12822–12834.
43 H.-Y. Yang, H.-B. Du, Y.-P. Bai, Y.-H. Ding, Y.-F. Ma, G. Wu, N. Zhang, N. K. Szymczak and S. Guo, *Sci. Adv.*, 2025, **11**, eadw8408.
44 C. Ye, G. L. Gard, R. W. Winter, R. G. Syvret, B. Twamley and J. n. M. Shreeve, *Org. Lett.*, 2007, **9**, 3841–3844.
45 P. Paquin, N. DeGrâce, G. Bélanger-Chabot and J.-F. Paquin, *J. Org. Chem.*, 2024, **89**, 3552–3562.
46 L. C. Peyrical, L. Vinet, E. Azek and A. B. Charette, *Org. Lett.*, 2024, **26**, 10414–10418.
47 N. M. Shavaleev, G. Xie, S. Varghese, D. B. Cordes, A. M. Z. Slawin, C. Momblona, E. Ortí, H. J. Bolink, I. D. W. Samuel and E. Zysman-Colman, *Inorg. Chem.*, 2015, **54**, 5907–5914.
48 P. Kenyon and S. Mecking, *J. Am. Chem. Soc.*, 2017, **139**, 13786–13790.
49 M. Talavera, S. Hinze, T. Braun, R. Laubenstein and R. Herrmann, *Molecules*, 2020, **25**, 3977.
50 R. D. W. Kemmitt, R. D. Peacock and J. Stocks, *J. Chem. Soc. D*, 1969, 554a–554a.
51 D. Langford, I. Göttker-Schnetmann, F. P. Wimmer, L. A. Casper, P. Kenyon, R. F. Winter and S. Mecking, *Organometallics*, 2019, **38**, 2710–2713.
52 M. Vanga, B. T. Diroll, A. Muñoz-Castro, A. Boretskyi, P. Mykhailiuk and H. V. R. Dias, *Inorg. Chem.*, 2025, DOI: 10.1021/acs.inorgchem.5c03702.
53 A. F. Henwood, J. Webster, D. Cordes, A. M. Z. Slawin, D. Jacquemin and E. Zysman-Colman, *RSC Adv.*, 2017, **7**, 25566–25574.
54 H. R. A. Golf, H.-U. Reissig and A. Wiehe, *J. Org. Chem.*, 2015, **80**, 5133–5143.
55 L. J. Sæthre, N. Berrah, J. D. Bozek, K. J. Børve, T. X. Carroll, E. Kukk, G. L. Gard, R. Winter and T. D. Thomas, *J. Am. Chem. Soc.*, 2001, **123**, 10729–10737.
56 R. Kordnezhadian, B.-Y. Li, A. Zogu, J. Demaerel, W. M. De Borggraeve and E. Ismalaj, *Chem. – Eur. J.*, 2022, **28**, e202201491.
57 H. V. R. Dias and C. J. Lovely, *Chem. Rev.*, 2008, **108**, 3223–3238.
58 A. Jalil, E. E. Happel, L. Cramer, A. Hunt, A. S. Hoffman, I. Waluyo, M. M. Montemore, P. Christopher and E. C. H. Sykes, *Science*, 2025, **387**, 869–873.
59 T. Pu, H. Tian, M. E. Ford, S. Rangarajan and I. E. Wachs, *ACS Catal.*, 2019, **9**, 10727–10750.
60 M. O. Ozbek, I. Onal and R. A. van Santen, *J. Catal.*, 2011, **284**, 230–235.
61 D. J. Safarik and R. B. Eldridge, *Ind. Eng. Chem. Res.*, 1998, **37**, 2571–2581.
62 R. B. Eldridge, *Ind. Eng. Chem. Res.*, 1993, **32**, 2208–2212.
63 Y. Ren, X. Liang, H. Dou, C. Ye, Z. Guo, J. Wang, Y. Pan, H. Wu, M. D. Guiver and Z. Jiang, *Adv. Sci.*, 2020, **7**, 2001398.
64 B. M. Binder, *J. Biol. Chem.*, 2020, **295**, 7710–7725.
65 E. M. Beyer Jr., *Plant Physiol.*, 1976, **58**, 268–271.
66 M. E. Saltveit, K. J. Bradford and D. R. Dilley, *J. Am. Soc. Hortic. Sci.*, 1978, **103**, 472–475.
67 T. Ziegler and A. Rauk, *Inorg. Chem.*, 1979, **18**, 1558–1565.
68 D. M. P. Mingos, *J. Organomet. Chem.*, 2001, **635**, 1–8.
69 H. V. R. Dias, D. Parasar, A. A. Yakovenko, P. W. Stephens, Á. Muñoz-Castro, M. Vanga, P. Mykhailiuk and E. Slobodyanyuk, *Chem. Sci.*, 2024, **15**, 2019–2025.
70 I. Krossing and A. Reisinger, *Angew. Chem., Int. Ed.*, 2003, **42**, 5725–5728.
71 H. V. R. Dias and J. Wu, *Eur. J. Inorg. Chem.*, 2008, **2008**, 509–522.
72 H. V. R. Dias, in *Comprehensive Coordination Chemistry II*, ed. J. A. McCleverty and T. J. Meyer, Pergamon, Oxford, 2003, pp. 383–463, DOI: 10.1016/B0-08-043748-6/02003-X.
73 M. M. Melero, Z. Kłosek, C. Ramírez de Arellano and A. Olmos, *J. Org. Chem.*, 2023, **88**, 9130–9135.
74 M. Kitamura, Y. Takenaka, T. Okuno, R. Holl and B. Wünsch, *Eur. J. Inorg. Chem.*, 2008, **2008**, 1188–1192.
75 M. Vanga, V. Q. H. Phan, J. Wu, A. Munoz-Castro and H. V. R. Dias, *Inorg. Chem.*, 2023, **62**, 18563–18572.
76 J. H. W. LaFortune, B. F. Jacobs and C. L. B. Macdonald, in *Comprehensive Coordination Chemistry III*, ed. E. C. Constable, G. Parkin and L. Que Jr, Elsevier, Oxford, 2021, pp. 214–280, DOI: 10.1016/B978-0-08-102688-5.00029-5.
77 C. J. Allan and C. L. B. MacDonald, *Comprehensive Inorganic Chemistry II: From Elements to Applications*, 2nd edn, 2013, vol. 1, pp. 485–566.
78 P. Ghosh, P. J. Desrosiers and G. Parkin, *J. Am. Chem. Soc.*, 1998, **120**, 10416–10422.

79 R. Han, P. Ghosh, P. J. Desrosiers, S. Trofimenko and G. Parkin, *J. Chem. Soc., Dalton Trans.*, 1997, 3713–3718.
80 C. Janiak, *Main Group Met. Chem.*, 1998, **21**, 33–50.
81 M. R. Biscoe, C. Uyeda and R. Breslow, *Org. Lett.*, 2004, **6**, 4331–4334.
82 C. Chen and R. F. Jordan, *Organometallics*, 2010, **29**, 3679–3682.
83 H. Schmidbaur, *Angew. Chem., Int. Ed. Engl.*, 1985, **24**, 893–904.
84 M. Bochmann, *Coord. Chem. Rev.*, 2009, **253**, 2000–2014.
85 H. V. R. Dias, S. Singh and T. R. Cundari, *Angew. Chem., Int. Ed.*, 2005, **44**, 4907–4910.
86 S. Alvarez, *Dalton Trans.*, 2013, **42**, 8617–8636.
87 B. Cordero, V. Gómez, A. E. Platero-Prats, M. Revés, J. Echeverría, E. Cremades, F. Barragán and S. Alvarez, *Dalton Trans.*, 2008, 2832–2838.
88 C. R. Groom, I. J. Bruno, M. P. Lightfoot and S. C. Ward, *Acta Crystallogr., Sect. B*, 2016, **72**, 171–179.
89 A. Bondi, *J. Phys. Chem.*, 1964, **68**, 441–451.
90 A. L. Rheingold, L. M. Liable-Sands and S. Trofimenko, *Chem. Commun.*, 1997, 1691–1692, DOI: 10.1039/a703349d.
91 W. Uhl, *Adv. Organomet. Chem.*, 2004, **51**, 53–108.
92 P. Ghosh, A. L. Rheingold and G. Parkin, *Inorg. Chem.*, 1999, **38**, 5464–5467.
93 H. V. R. Dias and J. Thankamani, *Acta Crystallogr., Sect. C: Cryst. Struct. Commun.*, 2013, **69**, 959–962.
94 C. Dowling, P. Ghosh and G. Parkin, *Polyhedron*, 1997, **16**, 3469–3473.
95 E. R. Sirianni, G. P. A. Yap and K. H. Theopold, *Inorg. Chem.*, 2014, **53**, 9424–9430.
96 K. L. V. Mann, J. C. Jeffery, J. A. McCleverty and M. D. Ward, *Polyhedron*, 1999, **18**, 721–727.
97 T. Fillebeen, T. Hascall and G. Parkin, *Inorg. Chem.*, 1997, **36**, 3787–3790.
98 C. Chen, H. Lee and R. F. Jordan, *Organometallics*, 2010, **29**, 5373–5381.
99 L. Falivene, Z. Cao, A. Petta, L. Serra, A. Poater, R. Oliva, V. Scarano and L. Cavallo, *Nat. Chem.*, 2019, **11**, 872–879.
100 L. Falivene, R. Credendino, A. Poater, A. Petta, L. Serra, R. Oliva, V. Scarano and L. Cavallo, *Organometallics*, 2016, **35**, 2286–2293.
101 L. Falivene, Z. Cao, A. Petta, L. Serra, A. Poater, R. Oliva, V. Scarano and L. Cavallo, *Nat. Chem.*, 2019, **11**, 872–879.
102 H. V. R. Dias and J. Wu, *Organometallics*, 2012, **31**, 1511–1517.
103 R. D. Vernet and V. Boekelheide, *Proc. Natl. Acad. Sci. U. S. A.*, 1974, **71**, 2961–2964.
104 A. B. Kazi, H. V. R. Dias, S. M. Tekarli, G. R. Morello and T. R. Cundari, *Organometallics*, 2009, **28**, 1826–1831.
105 D. V. Karade, V. Q. H. Phan and H. V. R. Dias, *Dalton Trans.*, 2024, **53**, 10426–10433.
106 B. T. Watson and H. V. R. Dias, *Chem. Commun.*, 2024, **60**, 4872–4889.
107 C. Elschenbroich, *Organometallics*, WILEY-VCH, Weinheim, 3rd edn, 2016.
108 A. Noonikara-Poyil, A. Muñoz-Castro, A. Boretskyi, P. K. Mykhailiuk and H. V. R. Dias, *Chem. Sci.*, 2024, **15**, 1159–1161.
109 H. V. R. Dias, Z. Wang and W. Jin, *Inorg. Chem.*, 1997, **36**, 6205–6215.
110 A. Reisinger, N. Trapp, I. Krossing, S. Altmannshofer, V. Herz, M. Presnitz and W. Scherer, *Angew. Chem., Int. Ed.*, 2007, **46**, 8295–8298.
111 A. Noonikara-Poyil, S. G. Ridlen, I. Fernández and H. V. R. Dias, *Chem. Sci.*, 2022, **13**, 7190–7203.
112 M. M. Díaz-Requejo and P. J. Pérez, *Chem. Rev.*, 2008, **108**, 3379–3394.
113 H. V. R. Dias, R. G. Browning, S. A. Richey and C. J. Lovely, *Organometallics*, 2004, **23**, 1200–1202.
114 M. Álvarez, F. Molina and P. J. Pérez, *J. Am. Chem. Soc.*, 2022, **144**, 23275–23279.
115 N. B. Jayaratna, D. B. Pardue, S. Ray, M. Yousufuddin, K. G. Thakur, T. R. Cundari and H. V. R. Dias, *Dalton Trans.*, 2013, **42**, 15399–15410.
116 A. Caballero, E. Despagnet-Ayoub, M. M. Díaz-Requejo, A. Díaz-Rodríguez, M. E. González-Núñez, R. Mello, B. K. Muñoz, W.-S. Ojo, G. Asensio, M. Etienne and P. J. Pérez, *Science*, 2011, **332**, 835–838.
117 R. Gava, A. Olmos, B. Noverges, T. Varea, E. Álvarez, T. R. Belderrain, A. Caballero, G. Asensio and P. J. Pérez, *ACS Catal.*, 2015, **5**, 3726–3730.
118 K. Rangan, M. Fianchini, S. Singh and H. V. R. Dias, *Inorg. Chim. Acta*, 2009, **362**, 4347–4352.
119 C. J. Lovely, J. A. Flores, X. Meng and H. V. R. Dias, *Synlett*, 2009, 129–132.
120 J. Urbano, T. R. Belderraín, M. C. Nicasio, S. Trofimenko, M. M. Díaz-Requejo and P. J. Pérez, *Organometallics*, 2005, **24**, 1528–1532.
121 H. C. Brown and T. E. Cole, *Organometallics*, 1983, **2**, 1316–1319.
122 S. Galván-Arzate and A. Santamaría, *Toxicol. Lett.*, 1998, **99**, 1–13.
123 G. Sheldrick, *Acta Crystallogr., Sect. A: Found. Adv.*, 2015, **71**, 3–8.
124 G. Sheldrick, *Acta Crystallogr., Sect. C: Struct. Chem.*, 2015, **71**, 3–8.
125 O. V. Dolomanov, L. J. Bourhis, R. J. Gildea, J. A. K. Howard and H. Puschmann, *J. Appl. Crystallogr.*, 2009, **42**, 339–341.
126 (*a*) CCDC 2498963: Experimental Crystal Structure Determination, 2025, DOI: 10.5517/ccdc.csd.cc2pwcqp; (*b*) CCDC 2498964: Experimental Crystal Structure Determination, 2025, DOI: 10.5517/ccdc.csd.cc2pwcrq; (*c*) CCDC 2498965: Experimental Crystal Structure Determination, 2025, DOI: 10.5517/ccdc.csd.cc2pwcsr; (*d*) CCDC 2498966: Experimental Crystal Structure Determination, 2025, DOI: 10.5517/ccdc.csd.cc2pwcts; (*e*) CCDC 2498967: Experimental Crystal Structure Determination, 2025, DOI: 10.5517/ccdc.csd.cc2pwcvt; (*f*) CCDC 2498968: Experimental Crystal Structure Determination, 2025, DOI: 10.5517/ccdc.csd.cc2pwcwv; (*g*) CCDC 2504337: Experimental Crystal Structure Determination, 2025, DOI: 10.5517/ccdc.csd.cc2q1z2v.